InSAR constraints on the source parameters of the 2001 Bhuj earthquake

D. A. Schmidt[1] and R. Bürgmann[2]

Received 1 November 2005; revised 16 December 2005; accepted 23 December 2005; published 28 January 2006.

[1] We present InSAR results of the coseismic displacement field for the January 2001 Bhuj earthquake. Using InSAR data along multiple tracks, we determine the optimal source parameters of the earthquake. The deformation pattern is first modeled assuming uniform slip on an elastic dislocation. A grid search is used to constrain the source location and finiteness assuming a strike, rake, and dip consistent with seismic studies. An inversion for the distributed slip places oblique reverse slip at depth with strike-slip motion resolved at shallower depths. The estimated size of the event is M_w 7.6. Results also suggest that the postseismic response is minimal. **Citation:** Schmidt, D. A., and R. Bürgmann (2006), InSAR constraints on the source parameters of the 2001 Bhuj earthquake, *Geophys. Res. Lett.*, *33*, L02315, doi:10.1029/2005GL025109.

1. Introduction

[2] The 2001 Bhuj earthquake occurred along a blind thrust within the Kutch Rift basin of western India (Figure 1). Moment tensor solutions indicate that the earthquake was a reverse event along an east-west striking fault, and aftershock locations identify a south-dipping fault plane [*Bodin and Horton*, 2004; *Negishi et al.*, 2002]. This event represents a reactivation of a former normal fault formed within a failed rift zone due to contemporary north-south compression as India collides with southern Asia [*Biswas*, 1987]. The Bhuj event is particularly interesting because it provides an opportunity to study a rare, large intraplate earthquake.

[3] Source parameters for the event have largely been constrained by teleseismic seismograms [*Antolik and Dreger*, 2003; *Singh et al.*, 2004] and aftershock locations [*Bodin and Horton*, 2004]. Due to the event's remote location, no strong motion and minimal geodetic data are available within the epicentral region. The only useful geodetic data in the region are from a triangulation network last surveyed in the 19th century [*Chandrasekhar et al.*, 2004] and scattered GPS observations [*Jade et al.*, 2002]. To supplement the geodetic data, *Gahalaut and Bürgmann* [2004] examined satellite images to infer surface deformation from the change in the distribution of surface water. Our results provide a first glimpse at the coseismic deformation field for this event. In this report, we solve for the source parameters of the 2001 Bhuj earthquake using the available InSAR data.

2. InSAR Data

[4] Interferometry has proven difficult for the region because of low overall phase coherence and because of technical difficulties experienced by the ERS satellite. The source region is characterized by broad lowlands interrupted by isolated highlands. The lowlands remain incoherent due to flooding and vegetation growth in all but the shortest temporal baselines which prevents the measurement of deformation in the epicentral region. Additionally, much of the 2001 SAR data has proven useless following the loss of gyroscopes aboard the ERS-2 satellite in January 2001 [*European Space Agency*, 2001, 2002]. The stabilization of the orbital control by the European Space Agency has allowed us to interfere more recent SAR data with pre-earthquake data. The lack of SAR data in 2001 means that all coseismic interferograms of the event include the first year of any postseismic deformation. Additionally, we have only been able to make one interferogram using only post-seismic SAR acquisitions, although future ENVISAT data may help to resolve this.

[5] We were able to successfully process 8 differential interferograms that span the coseismic event (Table 1). We have also examined several pre-earthquake interferograms and found that many are contaminated by widespread atmospheric artifacts. SAR data were collected by the ERS1/2 satellite along two adjacent descending tracks and one ascending track (Figure 1). For the modeling, we focus on a set of three interferograms from different satellite tracks (Figure 2). Additional figures showing the other coseismic interferograms are included in the electronic supplement[1]. The phase is unwrapped and converted to relative range-change measurements as described in the following section. The data are sub-sampled by taking every 300th data point from a vector of phase values (resulting in ~900 samples per interferogram) to reduce the number of redundant data, and adjacent pixels are averaged to avoid outliers.

3. Determination of Source Parameters

[6] We perform a grid search for the optimal source parameters of the earthquake. The parameters explored include the event location, the fault plane orientation, source finiteness, and slip magnitude. The deformation pattern is modeled assuming uniform slip on an elastic dislocation [*Okada*, 1985]. A grid search was performed so that trade-

[1]Department of Geological Sciences, University of Oregon, Eugene, Oregon, USA.
[2]Department of Earth and Planetary Science, University of California, Berkeley, California, USA.

0094-8276/06/2005GL025109$05.00

[1]Auxiliary material is available at ftp://ftp.agu.org/apend/gl/2005GL025109.

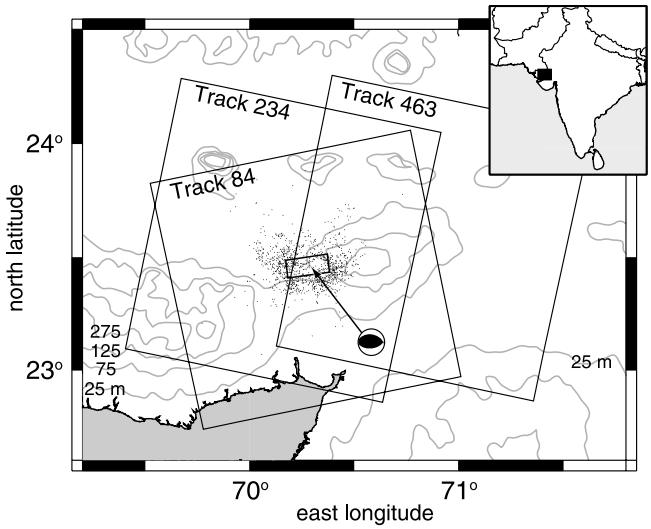

Figure 1. Regional map of the epicentral region in western India. Relocated aftershocks of *Bodin and Horton* [2004] are shown as black dots. Large black rectangles indicate the spatial coverage of the three ERS tracks along which SAR data were collected. The small rectangle indicates the surface projection of the preferred fault plane of Table 2. The mainshock focal mechanism (shifted from the epicenter) is taken from *Antolik and Dreger* [2003]. Elevation contours (gray lines) are in 50 m intervals.

offs in model parameters could be fully explored. For each perturbation in the parameter space, a forward calculation is performed and the predicted surface displacements are projected onto the satellite's line-of-sight. Since the look angle varies across a SAR scene, a variable unit vector is used for each track. The coherent InSAR phase is limited to the discontinuous highlands within each frame. Therefore, the absolute jump in phase is unknown between patches. For each iteration of the grid search, the modeled range-change is subtracted from the data, and the residual is minimized by inverting for the phase ambiguity between coherent patches and the orbital gradient across each interferogram. The residual sum of squares (RSS) is used to asses the fit to the data,

$$RSS = \sum_{i=1}^{N} \sum_{j=1}^{O_i} \left(\mathbf{R}_{ij} - \mathbf{u}_{ij}\mathbf{G}_j\mathbf{s} - \mathbf{F}_{ij}\mathbf{m}_{ij}\right)^2, \qquad (1)$$

given N interferograms with O pixels for a given interferogram. $\mathbf{R}_{ij}$ is the observed range-change in interferogram i at pixel j. The static Green's function $\mathbf{G}$ is used to predict the surface displacements given the strike-slip and dip-slip fault offset vector s, which is projected onto the satellite's line-of-sight with unit vector $\mathbf{u}$. The model parameters defining the offsets between InSAR patches and the slope across each interferogram are contained in vector $\mathbf{m}$ and related to the data with design matrix $\mathbf{F}$.

[7] The RSS is calculated for the full range of parameter values listed in Table 2. This allows us to explore all of the trade-offs and limitations when constraining the parameters of the event. There is a trade-off between the strike and dip where the data can be equally fit if the strike rotates northward as the dip increases. Unbounded models prefer dips greater than 60° for strikes less than 50°, although these values are physically unreasonable given the aftershock distribution and the geology. Solutions are influenced by the steep range-change gradient in the Wagad highlands directly east of the epicenter. We favor higher strikes and assume a strike of 82° and a dip of 51°. These values were adopted from the moment tensor solution of *Antolik and Dreger* [2003] and are consistent with the trade-off curve between these variables (see supplemental materials for figures of parameter trade-offs).

[8] Additionally, reverse and left-lateral strike-slip mechanisms are difficult to discriminate based on the InSAR data due to the lack of coherence in the epicentral region. Both mechanisms predict a decrease in range-change in the Wagad highlands. For a strike-slip mechanism, eastward displacement and uplift in the southeast quadrant would produce a decrease in range to the east, as would the uplift from a reverse mechanism. InSAR data near the epicenter would constrain the rake if the interferograms were coherent in this region. A subtle tapering in range-change observed on the east margin of the southwest coherent patch (see the circle in Figure 2a) is the only hint that a reverse mechanism is more appropriate, but the feature is not significant enough to control the optimization. The ambiguity of the rake is caused by how the three-dimensional surface displacements are mapped onto the satellite's line-of-sight.

[9] To overcome this ambiguity, we fix the rake at 77° as determined by *Antolik and Dreger* [2003] and optimize the remaining parameters. We find that the data are best fit by a planar dislocation extending from a depth of 15.1 km to 26.0 km. The along-strike length is optimized at 20.5 km and the slip magnitude is found to be 14.8 m which corresponds to 3.3 m of left-lateral slip and 14.4 m of reverse slip. The eastern edge of the fault plane is tightly constrained while the InSAR data is less sensitive to the placement of the western edge. Based on these preferred source parameters, the geodetically-inferred seismic moment is 1.9×10^{20} Nm, corresponding to a M_w7.5 earth-

Table 1. List of Coseismic Interferograms Processed[a]

ERS Track	Date YYYMMDD	Satellite Orbit	Date YYYMMDD	Satellite Orbit	Perp.
234	19960410	1-24771	20020214	2-35659	117 m
234	19960411	2-5098	20020214	2-35659	9[b]
234	19960516	2-5599	20020214	2-35659	19
234	19990401	2-20629	20010719	2-32653	494
234	19990506	2-21130	20020214	2-35659	188
84	19980827	2-17974	20020901	2-38515	30[b]
463	19990313	2-20357	20020928	2-38894	319
463	20000506	2-26369	20020928	2-38894	310[b]

[a]Supplemental figures show those interferograms not displayed in Figure 2.
[b]Interferograms used in the modeling.

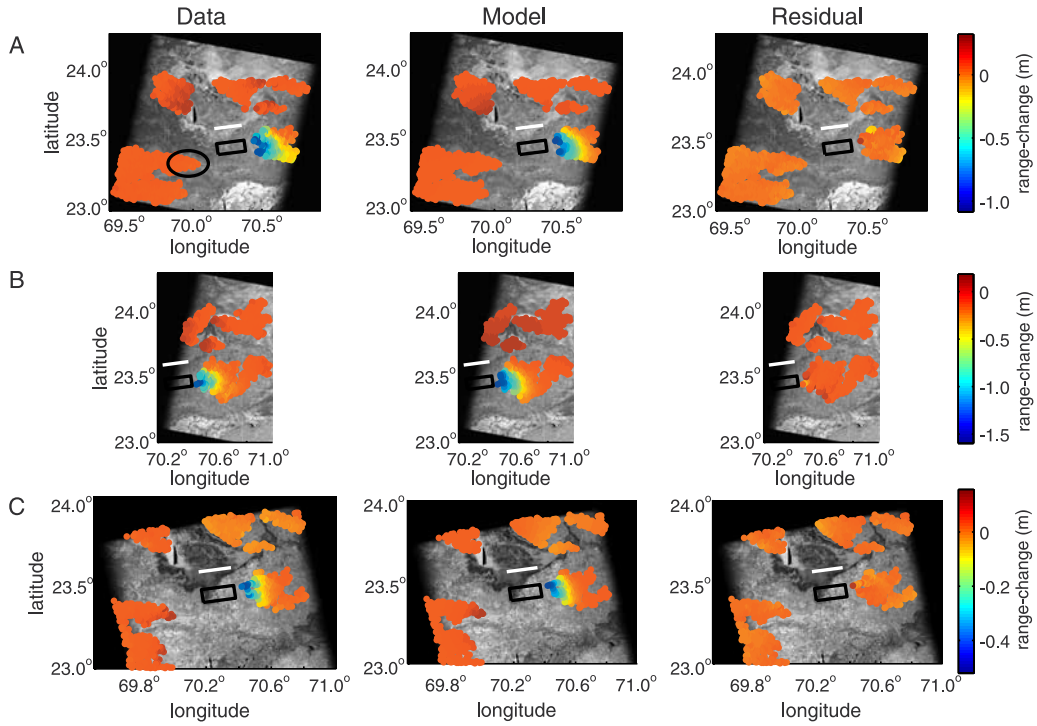

Figure 2. (left) InSAR data, (middle) estimated data for the model of distributed slip, and (right) data residual for the three interferograms: (a) 19960411-20020214, (b) 20000506-20020928, and (c) 19980827-20020901. The bold rectangle represents the surface projection of the fault plane listed in Table 2, and the white line marks the intersection of the fault plane with the surface. We find that reverse and strike-slip mechanism produce similar rang-change patterns. However the lack of an increase in range-change in the circled region (top left) indicates an oblique-thrust event.

quake with an assumed rigidity of 45 GPa. This set of parameters has a RSS of 4.0 m^2.

[10] If the a priori constraints on the rake, strike, and dip are relaxed then a global minimum (RSS = 3.5 m^2) is found with a dip-slip and strike-slip components of 2 m and 14 m, respectively, and a fault plane that extends between a depth of 9 km and 24 km. The corresponding along-strike length is 12 km. Examination of the parameter space reveals that as the rake rotates toward a more strike-slip solution, the dimensions of the fault plane systematically change such that the length decreases while the down-dip width and slip magnitude increase. However, these source parameters seem unreasonable given the focal mechanism of the main shock and the tectonic setting. Although this set of parameters produces a lower data misfit (RSS), we prefer those values found assuming a rake of 77° (Table 2).

4. Distributed Slip Model

[11] An inversion for a distributed slip model is performed using the preferred fault plane geometry listed in Table 2. The down-dip width and along-strike length of the fault plane are extended so that its dimensions are 35 km by 40 km, respectively, and the fault plane is discretized into square subfaults with a dimension of 4 km. The system of equations relating the data to the model parameters is described by

$$[\,\mathbf{uG}\;\;\mathbf{F}\,]\begin{bmatrix}\mathbf{s}\\ \mathbf{m}\end{bmatrix}=\mathbf{R}, \tag{2}$$

where the variables correspond to those defined in equation (1). The model parameters are optimized using a bounded least squares inversion that minimizes the data misfit while constraining the left-lateral strike slip and reverse components between 0 and 20 m. A smoothing constraint is not imposed because the slip distribution is found to be sufficiently smooth, likely due of the lack of near-source data which also limits the resolution of fine detail in the source.

[12] The estimated slip distribution is found to be relatively simple in that the inversion resolves one continuous patch (Figure 3). The rake is oblique reverse near the centroid and becomes strike-slip at shallower depths, especially in the northwest quadrant of the fault plane. The geodetically-inferred seismic moment for the slip distribution is 2.5 × 10^{20} Nm corresponding to a M_w 7.6 event. The RSS for the distributed slip model is 3.5 m^2.

Table 2. Range of Model Parameters Explored in a Grid Search for a Planar Dislocation With Uniform Slip[a]

Parameter	Minimum	Maximum	Preferred Model
Longitude,[b] deg	70.0	70.6	70.2822 ± 0.0003
Latitude,[b] deg	23.2	23.7	23.4203 ± 0.0005
Depth,[b] km	20	35	26.0 ± 1.1
Strike,[a] deg	0	180	82 ± 3
Dip,[a] deg	0	90	51 ± 1
Width, km	5	40	14.0 ± 0.2
Length, km	5	40	20.5 ± 0.4
Rake,[a] deg	0	90	77 ± 16
Slip, m	5	20	14.8 ± 0.8

[a]Strike, dip, and rake are adopted from the focal mechanism of *Antolik and Dreger* [2003].
[b]The longitude, latitude, and depth define the center of the lower edge.

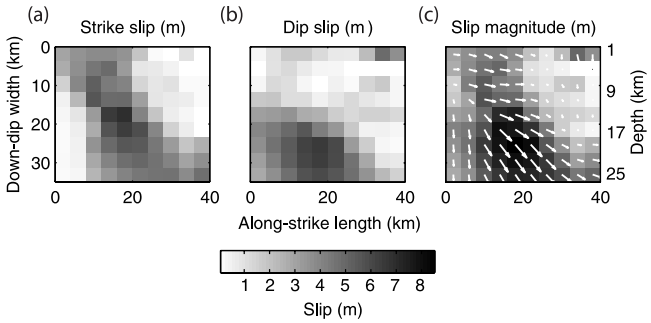

Figure 3. (a) Strike slip, (b) dip slip, and (c) oblique slip distribution on a south-dipping fault from the distributed slip inversion of the three interferograms shown in Figure 2. The fault plane is oriented such that right is to the east.

5. Discussion and Conclusions

[13] Our model results are consistent with a relatively deep, compact earthquake on an east-west striking, south-dipping fault. A grid search for the fault geometry places the dislocation relatively deep. The inferred fault plane lies entirely within the cloud of aftershocks relocated by *Bodin and Horton* [2004] and *Negishi et al.* [2002] which provides an independent test of the solution. The distributed slip model places the majority of slip within a 20×20 km^2 region centered at a depth of ~20 km. Our inversion result is consistent with the distributed slip model of *Antolik and Dreger* [2003] who found a deep slip patch from the inversion of teleseismic waveform data. They found that the majority of moment release occurred between a depth of 12 km and 25 km and the waveform data can be well fit by a simple point source model. Rupture directivity from their model was upward and to the northwest, consistent with a rupture that begins in the center of our model fault and propagates to the upper left corner (Figure 3).

[14] While we find oblique reverse slip near the event's centroid, a patch of strike-slip motion is resolved above a depth of 10 km. *Antolik and Dreger* [2003] found a secondary patch in the shallow subsurface from their inversion. However they assumed a constant oblique rake of 77° over the entire fault plane and did not explore whether this secondary patch could have had a different rake. While attempting to constrain shallow slip with leveling data, *Chandrasekhar et al.* [2004] found that strike-slip motion dominated on a shallow fault for a model composed of 2 planar dislocations.

[15] *Wesnousky et al.* [2001] reported no evidence of surface rupture in the field consistent with the observations from satellite imagery by *Gahalaut and Bürgmann* [2004]. This suggests that the event occurred on a blind thrust. While InSAR has been successfully used to map surface rupture for other earthquakes, the lack of InSAR coherence near the epicenter prevents us from confirming the absence of surface rupture. While slip is resolved near the top of the fault for the distributed slip model, we find that the InSAR data do not place a strong constraint on near-surface slip.

[16] We are unable to separate the coseismic deformation from any postseismic signal during the first year. However, we find the magnitude of the coseismic event as constrained by the InSAR data, which includes deformation in the first year following the coseismic event, is consistent with the magnitude estimated from seismic studies. Additionally, the examination of one postseismic interferogram (20020214-20040219) did not reveal any deformation greater than ~5 mm of range-change. This is consistent with a very small amount of postseismic deformation measured with GPS in the months following the earthquake [*Jade et al.*, 2002]. The agreement between the InSAR-derived and seismic-derived estimates of the seismic moment and the lack of postseismic signal after 2002 suggest that any postseismic response must be small in magnitude. This conclusion is not surprising given the fact that the earthquake occurred in an intraplate environment where the aseismic-seismic transition is sufficiently deep so as not to excite rapid postseismic relaxation of the lower crust or upper mantle [*To et al.*, 2004].

[17] **Acknowledgments.** Helpful comments were provided by an anonymous reviewer and Paul Bodin. Differential interferograms are produced using the software package ROI_PAC. The topographic contribution to the phase is removed using a digital elevation model from the Shuttle Radar Topography Mission. SAR data was obtained from ESA through Data Grant A03-330.

References

Antolik, M., and D. Dreger (2003), Rupture process of the 26 January 2 001 *Mw* 7.6 Bhuj, India, earthquake from teleseismic broadband data, *Bull. Seismol. Soc. Am.*, *93*, 1235–1248.

Biswas, S. K. (1987), Regional tectonic framework, structure and evolution of the western marginal basins of India, *Tectonophysics*, *135*, 302–327.

Bodin, P., and S. Horton (2004), Source parameters and tectonic implications of aftershocks of the *Mw* 7.6 Bhuj earthquake of 26 January 2001, *Bull. Seismol. Soc. Am.*, *94*, 818–827.

Chandrasekhar, D. V., D. C. Mishra, B. Singh, V. Vijayakumar, and R. Bürgmann (2004), Source parameters of the Bhuj earthquake, India, of January 26, 2001 from height and gravity changes, *Geophys. Res. Lett.*, *31*, L19608, doi:10.1029/2004GL020768.

European Space Agency (2001), Project News: ERS, *ESA Earth Obs. Q.*, *69*, 4.

European Space Agency (2002), Project News: ERS, *ESA Earth Obs. Q.*, *70*, 4.

Gahalaut, V. K., and R. Bürgmann (2004), Constraints on the source parameters of the 26 January 2001 Bhuj, India, earthquake from satellite images, *Bull. Seismol. Soc. Am.*, *94*, 2407–2413.

Jade, S., M. Mukul, I. A. Parvez, M. B. Anada, P. D. Kumar, and V. K. Gaur (2002), Estimates of coseismic displacement and post-seismic deformation using Global Position System geodesy for the Bhuj earthquake of 26 January 2001, *Curr. Sci.*, *82*, 748–752.

Negishi, H., J. Mori, T. Sato, R. Singh, S. Kumar, and N. Hirata (2002), Size and orientation of the fault plane for the 2001 Gujarat, India earthquake (M_w7.7) from aftershock observations: A high stress drop event, *Geophys. Res. Lett.*, *29*(20), 1949, doi:10.1029/2002GL015280.

Okada, Y. (1985), Surface deformation due to shear and tensile faults in a half-space, *Bull. Seismol. Soc. Am.*, *75*, 1135–1154.

Singh, S. K., J. F. Pacheco, B. K. Bansal, X. Pérez-Campos, R. S. Dattatrayam, and G. Suresh (2004), A source study of the Bhuj, India, earthquake of 26 January 2001 (M_w 7.6), *Bull. Seismol. Soc. Am.*, *94*, 1195–1206.

To, A., R. Bürgmann, and F. Pollitz (2004), Postseismic deformation and stress changes following the 1819 Rann of Kachchh, India earthquake: Was the 2001 Bhuj earthquake a triggered event?, *Geophys. Res. Lett.*, *31*, L13609, doi:10.1029/2004GL020220.

Wesnousky, S. G., L. Seeber, K. T. Rockwell, V. Thakur, R. Briggs, S. Kumar, and D. Ragona (2001), Eight days in Bhuj: Field report bearing on surface rupture and genesis of the January 26, 2001 Republic Day earthquake of India, *Seismol. Res. Lett.*, *72*, 514–524.

R. Bürgmann, Earth and Planetary Science, University of California, 307 McCone Hall, Berkeley, CA 94720-4767, USA. (burgmann@seismo.berkeley.edu)

D. A. Schmidt, Department of Geological Sciences, 1272 University of Oregon, Eugene, OR 97403-1272, USA. (das@uoregon.edu)